THE ASTROPHYSICAL JOURNAL, 258:83–95, 1982 July 1

ON THE ORIGIN OF THE 1 keV DIFFUSE X-RAY BACKGROUND

J. A. NOUSEK, P. M. FRIED, W. T. SANDERS, AND W. L. KRAUSHAAR
Department of Physics, University of Wisconsin, Madison
Received 1981 September 4; accepted 1982 January 8

ABSTRACT

High galactic latitude data ($b < -15°$) from the Wisconsin soft X-ray sky survey are used to constrain simple geometric models for the source of the diffuse X-ray background at energies near 1 keV. Two extended enhanced features are apparent in the intensity maps. One is in Eridanus and one is in the direction of the galactic center. Away from these features, the sky is relatively uniform. The observed degree of isotropy is consistent with the model that the 0.5–1.2 keV background consists of an isotropic extragalactic component plus a thick disk galactic component. If an $11E^{-1.4}$ photons cm^{-2} s^{-1} sr^{-1} keV^{-1} spectrum is assumed for the extragalactic component, then a temperature of 2–3 $\times$ 10^6 K and an emission measure perpendicular to the galactic plane of 0.004 cm^{-6} pc are derived for the galactic component. A local and isotropically distributed source model is also consistent with the data, but is difficult to accommodate on physical grounds. Several other source distributions, such as a simple isotropic extragalactic component or a *spherical* galactic halo, are in conflict with the data.

Subject headings: X-rays: general — interstellar: matter — galaxies: Milky Way

I. INTRODUCTION

Much of the interest in the diffuse soft X-ray background has focused on the very softest X-rays, those below 1/4 keV. The most likely origin for these X-rays is thermal emission from a hot ($T \sim 10^6$ K) local (closer than $\sim$100 pc) interstellar gas (Williamson *et al.* 1974; Burstein *et al.* 1977; Sanders *et al.* 1977; Hayakawa *et al.* 1978; Stern and Bowyer 1979; Paresce and Stern 1981). Fried *et al.* (1980) present soft X-ray data from the southern galactic hemisphere in the form of intensity maps which span the energy interval 0.1–2 keV. They compare their lowest energy data (0.1–0.28 keV) to models of the local interstellar medium.

The soft X-ray background in the energy interval 0.5–1.2 keV has received much less attention, presumably because the relative contributions of galactic and extragalactic sources are so very difficult to determine (Bunner, Sanders, and Nousek 1979). At energies greater than 2 keV, the X-ray diffuse background is isotropic and presumably of extragalactic origin. An unabsorbed extrapolation of this isotropic spectrum to the 0.5–1.2 keV energy interval accounts for only $\sim$65% of the observed intensity. A million degree thermal spectrum that could produce the bulk of the diffuse X-rays with energy below 0.28 keV could contribute at most 5% of the observed 0.5–1.2 keV intensity. There must be an additional emitting component, possibly stellar X-ray sources or dispersed higher temperature gas, which supplies the remainder of this intensity. The goal of this paper is to study the spatial and spectral characteristics of the 0.5–1.2 keV diffuse X-rays and to infer the nature of the source of that intensity. Most of our considerations and conclusions are independent of whether the emission is from a dispersed hot gas or from hot gas in the coronae of stars. The contribution of stars, particularly M dwarfs, to the diffuse X-ray background has been discussed recently by Rosner *et al.* (1981).

II. DATA

The observations described here were taken during a series of five Aerobee 170 rocket flights. The experimental details are described in Fried *et al.* (1980). The X-ray detectors on each flight were two proportional counters with honeycomb collimation providing a 6°.5 FWHM response, one with a boron-coated window and the other with a predominantly carbon window.

The poor energy resolution intrinsic to the proportional counter at low energies motivates us to combine data from a range of pulse heights into broad bands. The difference in transmission characteristics of the two windows is the chief source of spectral information below 0.284 keV. The lowest pulse height range (0.06–0.35 keV) in the counter with the boron-coated window is known as the B band because the sensitivity of this band is dominated by the absorption characteristics of boron. Detection of a pulse in this band indicates that the X-ray energy lay between the lowest energy able to penetrate the window, $\sim$0.1 keV, and the boron K absorption edge at 0.188 keV. Similarly, a pulse in the lowest pulse height range (0.06–0.45 keV) of the carbon window counter, the C band, indicates the detection of an X-ray with energy between $\sim$0.1 and 0.284 keV.

At higher energy the response characteristics of the two counters are similar (see for example, Burstein *et al.* 1977) and the data from the two counters have been combined. Three higher energy maps of Fried *et al.* have been combined to produce a single map (Fig. 1) covering the pulse height interval of 0.5–1.2 keV (the MI band).

1982ApJ...258...83N

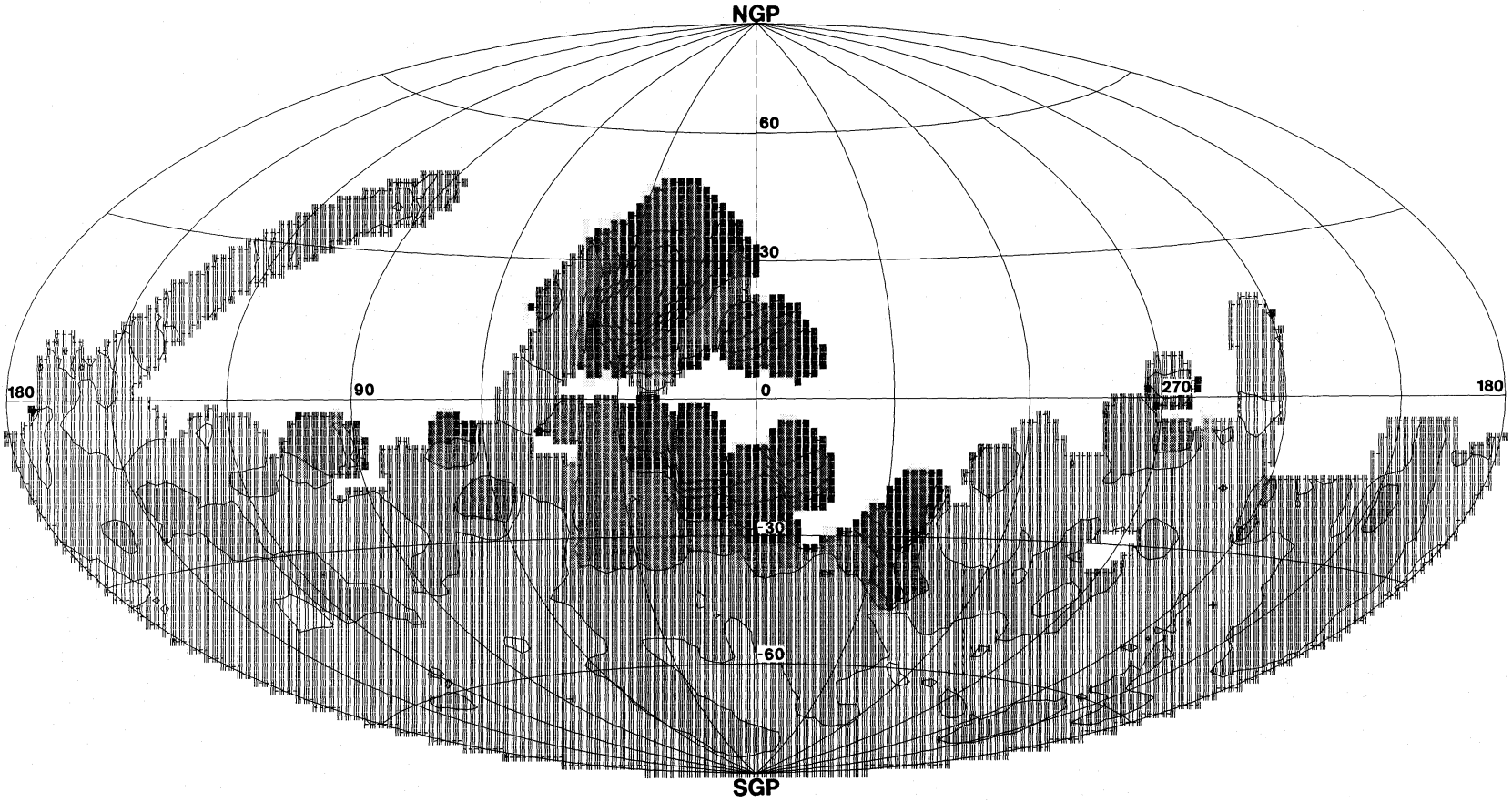

FIG. 1.—MI band (0.5–1.2 keV) intensity map in galactic coordinates. The shading is proportional to X-ray intensity: 1 line pixel^{-1} = 30 cts s^{-1} and 1 ct s^{-1} ~ 2.5 × 10^{-10} ergs cm^{-2} s^{-1} sr^{-1}. Near the center of the map the high-intensity regions are contoured without additional shading. Blank areas either were not viewed or have been eliminated because they contain X-ray sources bright in our 2–6 keV band.

Regions of high intensity are indicated by heavy shading. Each line per pixel of shading corresponds to 30 cts s^{-1} in the MI band, and 1 MI band ct s^{-1} corresponds to $\sim 2.5 \times 10^{-10}$ ergs cm^{-2} s^{-1} sr^{-1}, integrated over 0.5–1.2 keV, for a typical diffuse background spectrum. Near the center of the map the high intensity exceeds the dynamic range of the shading display, and the intensity is simply contoured without additional shading. Totally blank areas either were not viewed by the experiment or have been eliminated from the map because they contain X-ray sources bright in our 2–6 keV band. The blank region within 5°–10° of the galactic center and extending along the galactic plane as far as $l \sim 45°$ is one example of the latter. Fried *et al.* describe the map-making process in more detail. Data from the Crab, Vela, Puppis, and Cygnus Loop supernova remnants have also been eliminated, as have data from the sources in the Large Magellanic Cloud.

III. DISCUSSION OF THE MI BAND INTENSITY MAP

a) Galactic Center Region

The area within $\sim 40°$ of the galactic center direction is much more intense than the general sky brightness in the MI band. Within this area the observed intensity increases toward the direction of the galactic center, peaking at three times the general sky level. This enhancement is not the effect of low-energy "tails" of high energy point sources. Data taken while bright high-energy point sources were in the field of view were excluded, and similarly-prepared maps for the energy region 2–6 keV show no significant enhancement toward the galactic center. Furthermore, a sequence of observations of part of this region, using the *HEAO 2* X-ray telescope, shows no evidence for an increased number of point sources (Fried, Nousek, and Garmire 1982). Several local maxima give an uneven appearance to the region. Much of this structure may be due to foreground absorption or to our limited sky exposure close to strong point sources. It is likely that the bright features result from a single extended emission region. This may be the nearby (~ 150 pc) region that causes the North Polar Spur (NPS) features seen in radio continuum, H I, and 0.25 keV X-ray surveys. However, the greater extent of the MI band enhancement and the great penetration length of MI band X-rays leave open the possibility that some or all of the emission originates beyond the NPS.

The spectrum of the enhanced region does not vary strongly with position within the region. The pulse height data from three different areas of the enhanced region all can be well fitted using normal abundance thermal plasma emission models (Raymond and Smith 1979, hereafter RS) with $\log T = 6.47 \pm 0.07$, emission measures $n_e^2 d = 0.01$–0.03 cm^{-6} pc, and neutral absorbing gas consistent with N_H between 4×10^{20} cm^{-2} and 15×10^{20} cm^{-2}.

Hayakawa *et al.* (1977) assigned the enhanced intensity seen in this region to emission from a plasma inside the NPS with $\log T = 6.5$. At these energies and temperatures plasma emission is principally due to the lines of oxygen (0.57, 0.65 keV), iron (0.727, 0.812 keV), and neon (0.914 keV). Anomalous abundances of these elements or nonequilibrium effects in the plasma (Hayakawa *et al.* 1979) can reduce the emission measure required to explain the observed intensity. Our data from this region can also be well fitted by a spectrum consisting of only a few lines. The lines of both oxygen and neon are required for a good fit, but in no case does the addition of the iron lines improve the fit. The required ratio of the two oxygen lines is the same as found in collisional equilibrium at $\log T = 6.45$. These results are consistent with those of Inoue *et al.* (1980).

If the excess (over the general sky level) MI band emission in these directions originates in one uniform spherical region containing a solar abundance RS plasma at $\log T = 6.47$, then the pressure and thermal energy in this region are

$$P/k = 2 n_e T \sim 8 \times 10^5 \, d_{pc}^{-0.5} \text{ cm}^{-3} \text{ K} , \quad (1)$$

$$E_{TH} = 2.6 \times 10^{45} \, d_{pc}^{2.5} \text{ ergs} , \quad (2)$$

where d_{pc} is the diameter of the region in parsecs. If the enhanced region is associated with the NPS, then d_{pc} would be ~ 230 (Berkhuijsen 1973), and we would have $P/k \sim 5 \times 10^4$ cm^{-3} K and $E_{TH} \sim 2 \times 10^{51}$ ergs. These values are similar to those of Iwan (1980) for the NPS. If the enhancement is centered as far as the galactic center, then d_{pc} would be $\sim 10^4$, and we would have $P/k \sim 10^4$ cm^{-3} K and $E_{TH} \sim 10^{55}$ ergs. While this pressure is not unreasonable, the thermal energy is rather large.

b) Eridanus-Orion Region

Another enhanced MI band region is centered near $l \sim 205°$, $b \sim -30°$. The X-ray emission from this region has been analyzed as an evolved supernova remnant by Naranan *et al.* (1976). Heiles (1976) has interpreted 21 cm measurements of this region to indicate an expanding shell of neutral hydrogen centered at $l \sim 198°$, $b \sim -40°$. Reynolds and Ogden (1979) have studied Hα radiation from this region and find that ionized material extends from the Orion region ($b \sim -15°$) to the Eridanus region ($b \sim -45°$) with a spatial distribution very similar to the MI band feature discussed here. Reynolds and Ogden ascribe the Hα to recombination following excitation by ultraviolet radiation from the hot stars of the Orion association. For ultraviolet photons to travel from the Orion OB association to the Eridanus region requires a transparent medium such as would be provided by an old supernova cavity. If the Eridanus-Orion enhancement is an ancient SNR at the Orion association distance, the X-ray luminosity ($> 10^{35}$ ergs s^{-1}) is very high for its linear diameter ($\gtrsim 200$ pc). Seward *et al.* (1976) have reviewed the X-ray observations of supernova remnants and concluded that the X-ray luminosity appears to drop precipitously when the linear diameter becomes greater than about 50 pc. Theoretical calculations (e.g., Chevalier 1974) indicate that the initial supernova energy must be unusually large ($\gtrsim 10^{52}$ ergs) to leave a 200 pc remnant with a temperature high enough to produce a significant amount of MI band X-rays. An alternative model is that

of a supernova exploding in, and reheating, a cavity created by a previous supernova (Cox and Smith 1974) or by stellar winds (Weaver 1979). Such a picture was discussed by Heiles (1976) and was used by Borken and Iwan (1977) and Iwan (1980) to explain their North Polar Spur X-ray observations.

c) *Unenhanced Background Regions*

If the large Eridanus and galactic center features are excluded, the remaining half of the southern galactic hemisphere shows a reasonably isotropic MI band intensity distribution. This contrasts with the intensity distributions measured in the B and C bands. Figure 2 displays the MI band intensity as a function of N_H for 15° intervals of galactic latitude. Except for the count rates measured toward the galactic center and the Eridanus features (indicated by open circles), the data are all consistent with a count rate ~ 100 cts s^{-1} and show little or no systematic variation with N_H. In contrast, analogous plots for the B band and C band show intensity variations of up to a factor of 3, as well as a general anticorrelation with N_H (Sanders *et al.* 1977).

Because the intensity distribution of the MI band X-rays differs significantly from that of the B and C band X-rays, we argue against their common origin in an emitting region characterized by a single temperature. It is improbable that the temperature and emission measure of the local emitting region vary so as to provide a constant intensity in the MI band and still induce an anticorrelation between the B and C band rates and the distant neutral hydrogen. It is more likely that the local B band and C band emitting region contributes only a small fraction of the MI band X-rays. If the local gas is in collisional equilibrium at 10^6 K (RS models), that fraction is $\lesssim 5\%$. Other emission regions or mechanisms provide the bulk of the MI band X-rays.

There are problems in accommodating local (closer than ~ 100 pc) isotropic emission mechanisms. The high degree of isotropy of the MI band radiation would require the Sun to be located improbably near to the center of a local optically thin MI band emission region. A local emitting region could provide an isotropic MI band flux if most of the MI band flux were in resonance lines optically thick to scattering. However, even in the center of the O VIII 18.97 Å line, a distance of 100 pc through a gas with all oxygen in the O^{+7} state and with $n_e = 0.01$ cm^{-3} corresponds to a scattering optical depth less than unity. Furthermore, lines in the B band and C band would be scattered even more than those in the MI band. Another possibility is that the Sun could be surrounded by a shell of uniform MI band surface brightness. Since surface brightness is distance independent, there are no constraints on the location of the Sun or on the shape of the shell. However, the nonequilibrium models of Cox and Anderson (1982), which produce MI band X-rays near the edges of a blast-heated cavity, provide at most 10% of the observed MI band flux.

If the isotropic power law spectrum of the 2–10 keV diffuse background, 11 $E^{-1.4}$ photons cm^{-2} s^{-1} sr^{-1} keV^{-1} (Henry *et al.* 1971; Bunner *et al.* 1971), continued unabsorbed down to 0.5 keV, it would provide $\sim 65\%$ of the MI band intensity. Its contribution would be less than 65% and it would not appear isotropic, because absorption by galactic matter is appreciable in this energy range. The count rate produced by an 11 $E^{-1.4}$ spectrum after attenuation by galactic matter, using the cross sections of Brown and Gould (1970), is indicated by the solid line in Figure 2.

The next section discusses the limitations that our data place on the spatial distribution of the sources of the required MI band emission for several very simple models.

IV. SPATIAL STRUCTURE OF THE UNENHANCED MI BAND DIFFUSE BACKGROUND

The mean interstellar absorption cross section per hydrogen atom (Brown and Gould 1970) for the MI band is ~ 3–5×10^{-22} cm^2, depending on the incident X-ray spectrum. Thus the characteristic range of MI band X-rays is of order kiloparsecs, comparable to the scale of galactic structure. In this section we compare our observations to the predictions of several different models for the spatial distribution of the MI band emission. The models we consider are local isotropic emission, extragalactic isotropic emission, and spherical and disk-shaped galactic halos. We eliminate data taken when the center of the field of view was within 15° of the galactic plane, to reduce contributions from point sources and supernova remnants.

None of the models that we compare to our data yield a good fit as defined by a minimum χ^2 procedure. The 1199 individual 0.2 s data points (during which the rockets scanned $\lesssim 1°$) show more scatter (mean $\pm$s.d. $= 17.6 \pm 5.7$ cts) than would be expected from a truly isotropic distribution. This scatter, combined with the large number of data points, ensures that our simple models result in χ^2 probabilities < 0.001. This is expected because the models address the large-scale structure of the MI band diffuse background, but not small-scale variations. Our intent then is to convey a sense of the data—to identify those spatial distributions that the data most nearly resemble and to indicate which distributions the data do not resemble. We give the best fit parameter values (determined using a minimum χ^2 procedure) associated with each model, but do not attempt to define a range of acceptable parameter values.

We assume that at these galactic latitudes the 21 cm inferred column densities provide reasonable estimates of the MI band absorption. If they provide *overestimates* of the MI band absorption, the 25% MI band intensity variations expected from the N_H variations of 2–10×10^{20} cm^{-2} would be reduced. However, this alternative seems unlikely in that comparisons of X-ray absorption column densities to 21 cm measured values have found the X-ray values higher (Gorenstein 1975; Ride and Walker 1977). Optically thick clouds could reduce the X-ray absorption while preserving the observed 21 cm values, but the lack of small-scale struc-

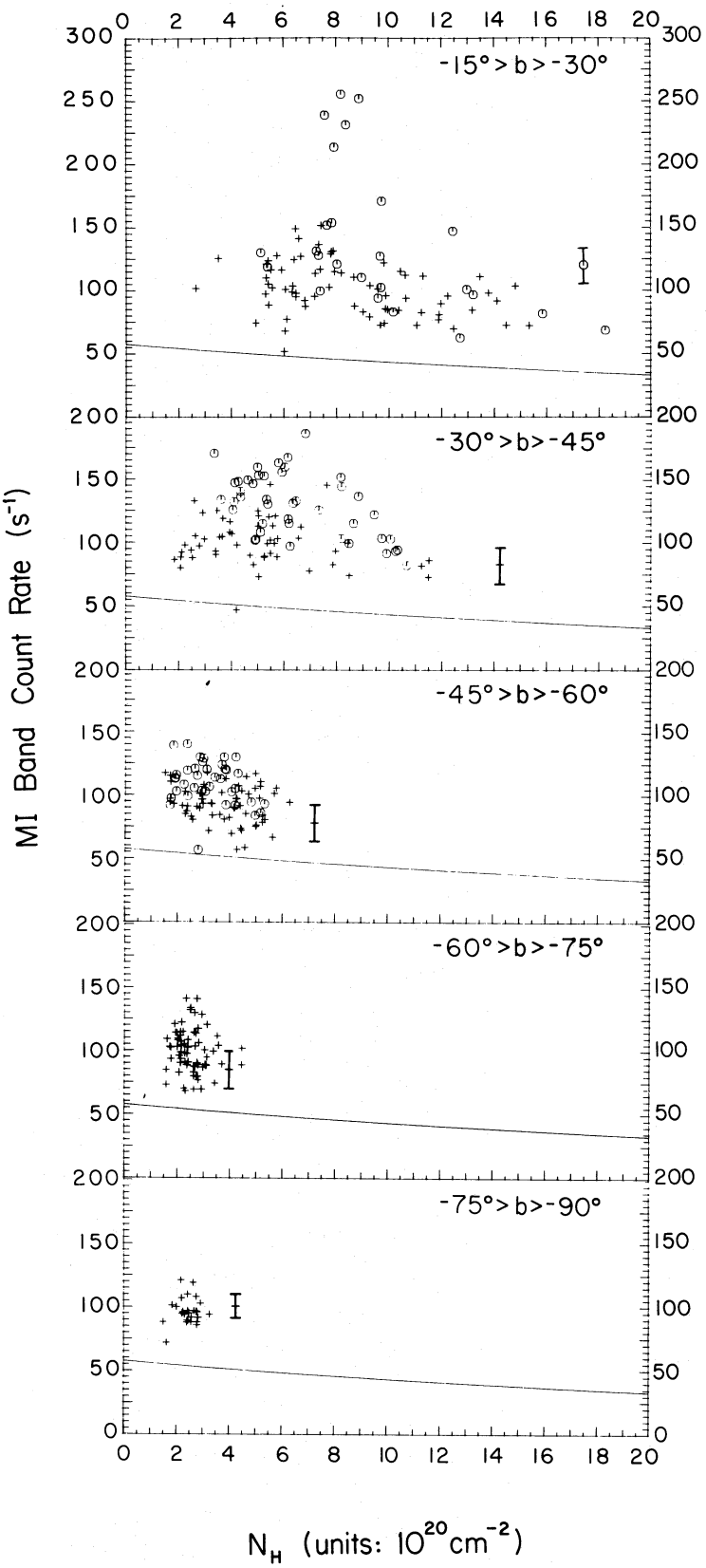

FIG. 2.—MI band intensity versus neutral hydrogen column density (Cleary, Heiles, and Haslam 1979) for several different galactic longitude intervals. The solid line indicates the calculated intensity from an 11 $E^{-1.4}$ photons $cm^{-2}\,s^{-1}\,sr^{-1}\,keV^{-1}$ extragalactic spectrum after absorption by neutral hydrogen. A typical 1 σ error bar is shown. Data points of less than 3 σ significance are not plotted.

ture found by Dickey, Salpeter, and Terzian (1979) at moderate to high galactic latitudes makes this an unlikely possibility.

a) *Model I: Isotropic*

We consider a model of the form

$$R_{\rm MI} = A + B \exp(-\sigma N_{\rm H}), \quad (3)$$

where $R_{\rm MI}$ is the observed MI band count rate, A is the count rate from an unabsorbed, local, isotropic component, and B is the count rate of an absorbed, extragalactic isotropic component. The best fit parameters to this model are $A = 92$ cts s^{-1}, $B = 0$, yielding a χ^2 per degree of freedom, χ^2/ν, of 1.38. This fit, the best produced by any we tried, suggests that the MI band spatial distribution is isotropic and shows no evidence for absorption by neutral gas. However, a very local origin for all of the MI band radiation, closer than the bulk of the neutral hydrogen, is difficult to accept for the reasons discussed in § III.

Since it seems that 21 cm measured $N_{\rm H}$ should be a good measure of the MI band absorption, we ask how much of the MI band intensity could be of extragalactic origin. If we fix B at the value appropriate for 11 $E^{-1.4}$ spectrum, $B = 58$ cts s^{-1}, then $\chi^2/\nu = 1.44$, slightly higher than for the isotropic unabsorbed model. In this case, however, an uncomfortably large isotropic (local) component, $A = 35$ cts s^{-1}, still must be explained. If we require there to be no local component, $A = 0$, then χ^2/ν rises to 1.69, clearly a much worse fit than the isotropic unabsorbed case.

An alternative interpretation of equation (3) is that of an absorbed extragalactic component, I_{Xg}, plus a galactic component, I_g, of which the emissivity is proportional to the neutral gas. In that case, we have the following expression (see Davidsen *et al.* 1972):

$$R_{\rm MI} = I_{Xg} \exp(-\sigma N_{\rm H}) + I_g[1 - \exp(-\sigma N_{\rm H})]$$
$$= I_g + (I_{Xg} - I_g) \exp(-\sigma N_{\rm H}). \quad (4)$$

Acceptable fits ($\chi^2/\nu \leq 1.44$) are achieved with $I_{Xg} = A + B \sim 93$ cts s^{-1} and $I_g = A \gtrsim 35$ cts s^{-1}. This value of I_{Xg} is $\sim 60\%$ greater than that provided by an extrapolation of the 11 $E^{-1.4}$ spectrum. $I_g > 35$ cts s^{-1} implies that $\xi/4\pi\sigma n_{\rm H} > 9 \times 10^{-9}$ ergs cm^{-2} s^{-1} sr^{-1} in the galactic plane, where ξ is the MI band volume emissivity. Assuming $n_{\rm H} \sim 1$ cm^{-3}, this constraint requires a source luminosity $\gtrsim 2 \times 10^{28}$ ergs s^{-1} if the sources are M stars (Allen 1973), or $n_e \gtrsim 0.002$ cm^{-3} if the source is distributed hot gas (RS models). Neither of these requirements would be particularly troublesome if there were some physical mechanism to distribute the emission with the absorbing neutral gas.

b) *Model II: Spherical Galactic Halo*

The predicted X-ray intensity at the Earth from a uniformly emitting sphere, centered at the galactic center, is

$$R_{\rm MI} = A[\cos\theta + (\rho^2 - \sin^2\theta)^{1/2}] \exp(-\sigma N_{\rm H}), \quad (5)$$

where ρ (assumed >1) is the ratio of the radius of the halo sphere to the Sun's galactic radius, and $\cos\theta = \cos(l)\cos(b)$. We consider in this model only the absorbed case because unabsorbed emission from a galactic halo is not physically reasonable. A spherical galactic halo model is a much poorer fit to our data than Model I with $A = 0$, unless ρ is so large ($\rho \gtrsim 20$) as to make the model effectively isotropic, and therefore the same as Model I. For example, if $\rho = 2$, χ^2/ν is 2.51; but if $\rho = 20$, χ^2/ν is 1.75.

Somewhat better fits can be achieved using a two-component model with one component the uniformly emitting sphere described above and the other component isotropic and unabsorbed. For $\rho = 2$, if the sphere component provides half the MI band counts, then χ^2/ν is 1.66, still not a very good fit. If this sphere component provides only one-tenth of the MI band counts, then χ^2/ν is reduced to 1.44 and this model approaches Model I with $B = 0$. Thus, a spherical galactic halo with $\rho > 1$ is consistent with our data only if its contribution is negligible.

A spherical galactic halo with $\rho < 1$ would produce a pronounced intensity enhancement toward the galactic center. As previously discussed, our southern galactic hemisphere data do show a general and pronounced intensity enhancement in the galactic center direction. Whether the MI band galactic center enhancement is a nearby feature or arises from distant emission that lies in the direction of a nearby feature cannot be determined from these data.

c) *Model III: Disklike Galactic Halo*

A simple unabsorbed disk model of the form $R_{\rm MI} = A/\sin|b|$ predicts spatial variations far too large to be consistent with the observed isotropy of the data ($\chi^2/\nu = 2.92$). The same model with absorption, $R_{\rm MI} = A \exp(-\sigma N_{\rm H})/\sin|b|$, more nearly fits the data ($\chi^2/\nu = 2.13$) because the increased emission for small $|b|$ is absorbed by the increased neutral material at low galactic latitudes. However, this model is still far from acceptable.

A model that does approximate the observed isotropy consists of a disklike halo plus an isotropic component, both absorbed by all of the neutral material along the line of sight. The model predicts

$$R_{\rm MI} = (A/\sin|b| + B) \exp(-\sigma N_{\rm H}), \quad (6)$$

where A measures the disklike galactic halo component and B the isotropic component. This model fits the data almost as well as the unabsorbed isotropic model ($\chi^2/\nu = 1.44$ for $A = 25$ cts s^{-1}, $B = 72$ cts s^{-1}). If B is forced to the value corresponding to an extrapolation of 11 $E^{-1.4}$, 58 cts s^{-1}, then $A = 35$ cts s^{-1} and $\chi^2/\nu = 1.46$.

A similar picture, which is not explicitly modeled here, is one studied by Davidsen *et al.* (1972)—a plane-parallel galactic X-ray emitting component with a half-thickness, z_s, greater than that of the neutral hydrogen, $z_{\rm H}$. They assumed the density of neutral hydrogen to be constant for $z < z_{\rm H}$ and zero elsewhere. If $z_s \sim z_{\rm H}$, this reduces to Model I, as discussed earlier (see eq. [4]). If z_s is signifi-

TABLE 1

SUMMARY OF SPATIAL MODELS

MODEL	ANALYTIC FORM	BEST FIT PARAMETERS[a] A (cts s^{-1})	B (cts s^{-1})	χ^2/ν
I	$A + B \exp(-\sigma N_H)$	92	0	1.38
	$A + B \exp(-\sigma N_H)$	35	(58)	1.44
	$B \exp(-\sigma N_H)$	...	109	1.69
II	$A[\cos\theta + (\rho^2 - \sin^2\theta)^{1/2}] \exp(-\sigma N_H)$, $\rho = 2$	75		2.51
	$A[\cos\theta + (\rho^2 - \sin^2\theta)^{1/2}] \exp(-\sigma N_H)$, $\rho = 20$	5.4		1.75
III	$(A/\sin\lvert b\rvert + B) \exp(-\sigma N_H)$	25	72	1.44
	$(A/\sin\lvert b\rvert + B) \exp(-\sigma N_H)$	35	(58)	1.46

[a] The parameter values in parentheses were not allowed to vary, but were fixed at the value appropriate for an 11 $E^{-1.4}$ spectrum.

cantly greater than z_H, then our Model III is a reasonable approximation for our purpose of conveying a sense of the data.

d) *Summary of Spatial Models*

In Table 1 we have summarized the results of our comparison of MI band spatial data with the predictions of several simple models. The spatial model for the general MI band diffuse background that most nearly resembles the data is that of an unabsorbed isotropic intensity. Two other models that resemble the data almost as well are two-component models of which the first component is an extragalactic 11 $E^{-1.4}$ spectrum. The second component in one case is local and isotropic and thus subject to the same objections as the single-component isotropic model. In the other two-component model, the second component is a disklike galactic halo absorbed by all the neutral material along the line of sight. There may be some support for this picture from the work of Savage and de Boer (1979, 1981), who present observational evidence for a hot gaseous galactic corona, or from that of Rosner *et al.* (1981), who discuss the evidence for a stellar (almost entirely dM star) contribution to the galactic soft X-ray background.

V. SPECTRAL CHARACTERISTICS OF THE MI BAND DIFFUSE RADIATION

In the preceding discussion of models for the source of the MI band diffuse radiation, only information as to the spatial distribution of the total intensity was used. In this section we use the spectral shape of the MI band intensity and its relation to the B and C bands to learn more of the characteristics of the emitting sources. The discussion in this section is independent of specific spectral models. Section VI compares the data to the equilibrium plasma emission models of Raymond and Smith (1979).

Burstein *et al.* (1977) suggested that the soft X-ray spectrum from 0.1 to 0.85 keV required emission from at least two different regions. In doing this they introduced the band-fraction diagram. This diagram displays the observed rates as ratios to the total rate, $R_T = R_B + R_C + R_M$, where R_B, R_C, and R_M are the rates in B (0.1–0.188 keV), C (0.1–0.284 keV), and M (0.5–0.85 keV) bands, respectively. The two ratios, $f_B(=R_B/R_T)$ and $f_M(=R_M/R_T)$, carry all of the spectral information available from these three bands. If two intrinsically different spectra contribute to an observation, the band-fraction point for the composite lies on a line connecting the band-fraction points for the two components. The position along this line is determined by weighting factors equal to the total rates for the individual components. Figure 3 shows our data from the southern galactic hemisphere, excluding the galactic center and Eridanus features, plotted on a f_M versus f_B (hereafter BCM) band-fraction diagram. Our data are similar to those of Burstein *et al.* from a smaller region of the sky.

A band-fraction analysis can also be applied to the 0.5–1.2 keV data by using the M_1 (0.5–0.65 keV), M_2 (0.65–0.85 keV), and I (0.85–1.2 keV) bands of Fried *et al.* (1980). If $R_{MI} = R_{M_1} + R_{M_2} + R_I$, where R_{M_1}, R_{M_2}, and R_I are the rates in the M_1, M_2, and I bands, respectively, then the appropriate fractions are $f_{M_1} = R_{M_1}/R_{MI}$ and $f_I = R_I/R_{MI}$. In Figure 4 the data from the southern galactic hemisphere, excluding center and Eridanus

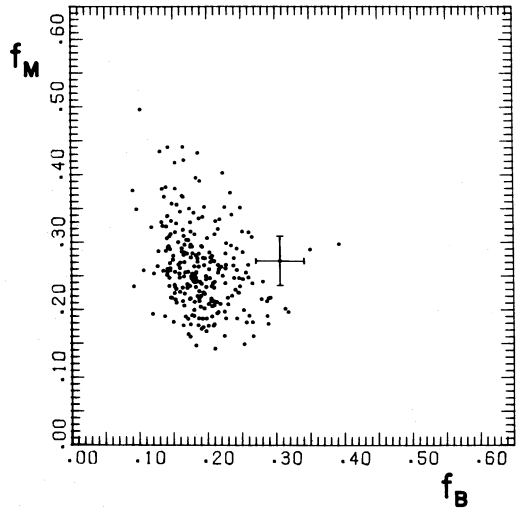

FIG. 3.—BCM band-fraction diagram for all data with $b < -15°$ outside of the galactic center and Eridanus features. A typical 1 σ error bar is shown. Data points of less than 3 σ significance are not plotted.

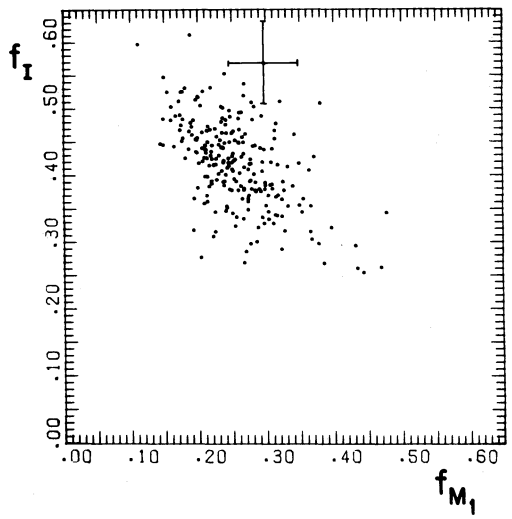

FIG. 4.—Same as Fig. 3, but for the MI band

features, are plotted on an f_I versus f_{M_1} (hereafter MI) band-fraction diagram.

Figure 5 shows band-fraction diagrams similar to those of Figures 3 and 4, but here each diagram shows data only for those regions of the sky where N_H has the restricted values indicated. N_H values are from Cleary, Heiles, and Haslam (1979). On the MI diagrams the mean positions of the data points show no pronounced dependency on N_H. On the BCM diagrams, on the other hand, there is a clear tendency for the data points to have mean positions that tend toward large values of f_M for large values of N_H. This qualitative feature of the data persists even if the extrapolated contribution from the extragalactic power law spectrum (11 $E^{-1.4}$) is subtracted.

These spectral data are consistent with the following simple model. Along every line of sight there is X-ray emission from two components. The "far" component originates beyond the galactic absorbing gas and is totally responsible for the intensity measured in our M_1, M_2, and I bands. The emitted spectrum of this more distant emission is constant over the sky and is characteristically hard so that most of the radiation is affected but little by the intervening galactic gas. Hence the MI band data are more or less constant in both intensity and spectral characteristics. The contribution from this distant emission would be represented on the MI band-fraction diagram by a point at $f_{M_1} = 0.25$, $f_I = 0.40$, independent of N_H. On the BCM band-fraction diagram it would correspond to a point near $f_B = 0.0$, $f_M = 0.5$ in directions of small N_H, and to a point near $f_B = 0.0$, $f_M = 0.7$ in directions of large N_H.

The "near" component originates closer than practically all the galactic absorbing gas and is responsible for almost all of the measured intensity in the B band, most of the C band, but almost none of the M band. The contribution from this region would then be represented by a point on the BCM band-fraction diagram at, for example, $f_B = 0.3$, $f_M = 0.0$. Since all measurements include contributions from both of these components, the resulting band-fraction points lie at weighted positions along the line connecting the individual component points discussed above. We know from previous studies (Sanders *et al.* 1977, for example) that the B and C band intensities anticorrelate with N_H. The anticorrelation with N_H of the near component, combined with the hardening with N_H of the far component, explains the general behaviour of the points on the BCM band-fraction diagram with changing N_H. The f_M of the far component increases with increasing N_H, while the weighting of the near component decreases with increasing N_H.

VI. COMPARISON OF OBSERVATIONS TO EQUILIBRIUM X-RAY EMISSION MODELS

The preceding discussion is independent of specific assumptions regarding the nature of the emission mechanisms. To estimate the physical parameters of the emitting regions we now assume that both emitting regions are hot RS plasmas in collisional ionization equilibrium. This assumption may not be valid. If the emission is from dispersed gas and this gas has been shock-heated (by supernova explosions, for example), the ionization states of the ions in the plasma may not have had time to reach collisional equilibrium with the electrons. The resulting X-ray spectrum can differ radically from the equilibrium case (Shapiro and Moore 1976; Hayakawa *et al.* 1979; Cox and Anderson 1982). Further, the spectrum may differ from the RS predictions if the elemental abundances differ from solar. We have found that reduced abundance of metals changes the spectral shape by a small amount, but reduces the plasma radiation efficiency by a large amount. Little is known about the emission spectrum from dM stars, the most likely significant stellar sources (Rosner *et al.* 1981). The parameter values that we derive here apply only insofar as the emissivity resembles that of a RS plasma in collisional equilibrium.

We have used data from two well-measured (high exposure) points located in high-latitude featureless regions of the sky. Table 2 gives the observed band rates from direction R ($l \approx 284°$, $b \approx -79°$) and direction T ($l \approx 70°$, $b \approx -45°$) as well as the calculated band rates from an 11 $E^{-1.4}$ spectrum absorbed by all the N_H along the line of sight.

The MI band-fraction point derived from the direction R data is plotted in Figure 6 along with the band-fraction points appropriate to RS model spectra, labeled by the logarithm of the temperature. Absorption by $N_H \lesssim 10 \times 10^{20}$ cm^{-2} affects the model and corresponding MI band-fraction points very little. (The inferred value of log T for a given band-fraction point decreases by <0.05 as N_H increases from 0 to 10^{21} cm^{-2}.) The location of the direction R data point is not consistent with a single-temperature RS model with $6.1 < \log T < 6.9$.

When the contribution of an 11 $E^{-1.4}$ extragalactic intensity, attenuated by $N_H = 3 \times 10^{20}$ cm^{-2}, the total N_H along the line of sight, is subtracted from the data,

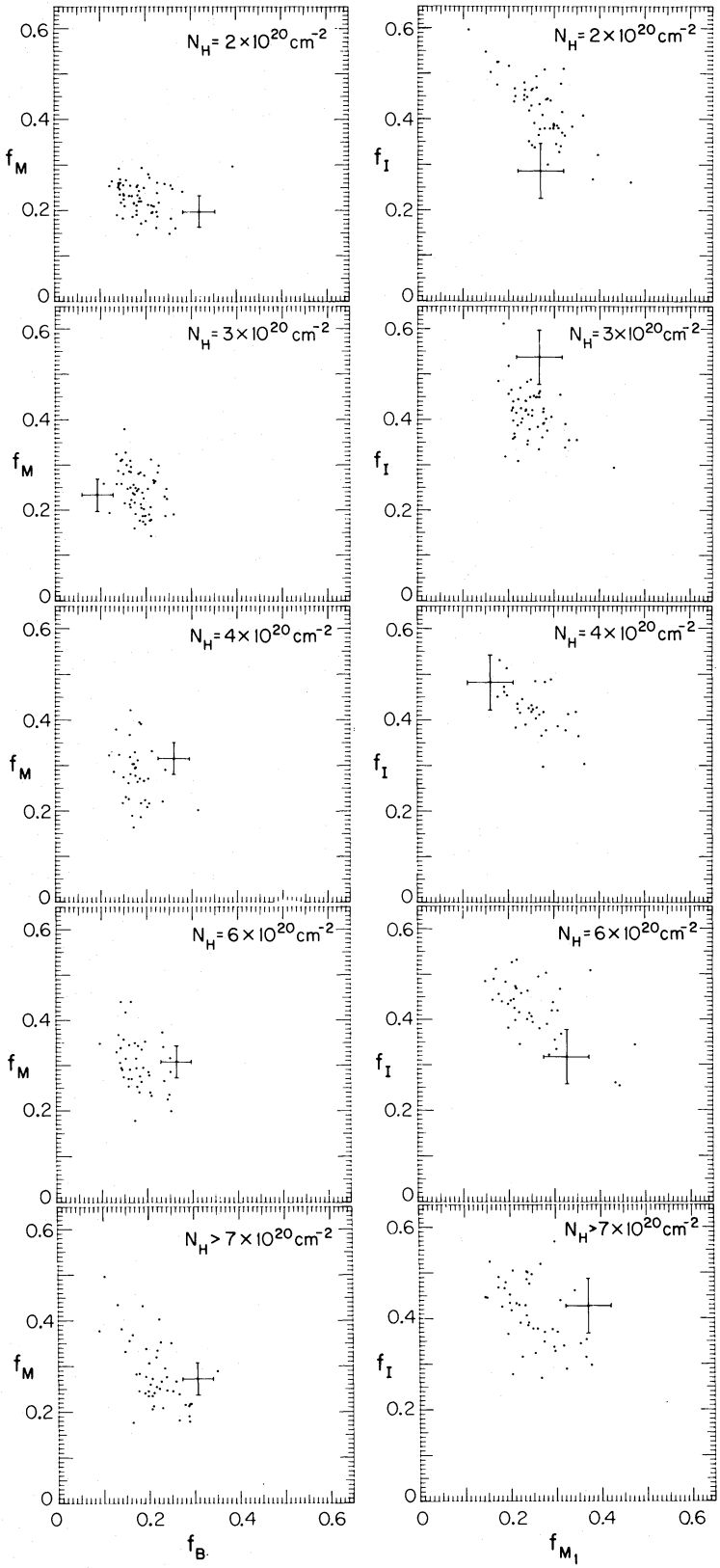

FIG. 5.—BCM (*left hand column*) and MI band-fraction diagrams for several different ranges of neutral hydrogen column density (Cleary, Heiles, and Haslam 1979). Typical 1 σ error bars are shown. Data points of less than 3 σ significance are not plotted.

TABLE 2

BAND RATES FROM TWO HIGH-LATITUDE POINTS

POINT	N_H (10^{20} cm^{-2})	DESCRIPTION	BAND RATES (cts s^{-1}) B	C	M_1	M_2	I
R	3	Observed from $l \sim 284°$, $b \sim -79°$	58.5 ± 2.4	167.6 ± 3.1	19.8 ± 1.4	29.6 ± 1.3	40.2 ± 1.4
		Calculated from absorbed 11 $E^{-1.4}$ spectrum	0.9	10.4	8.1	15.6	29.1
T	6	Observed from $l \sim 70°$, $b \sim -45°$	40.7 ± 5.4	99.4 ± 3.3	16.6 ± 1.2	26.2 ± 2.0	40.3 ± 1.8
		Calculated from absorbed 11 $E^{-1.4}$ spectrum	0.4	3.4	7.0	14.1	27.4

the resulting band-fraction point moves as indicated by the arrow in Figure 6. Perhaps fortuitously, after this correction the MI band-fractions agree with a single temperature plasma model with log $T = 6.4$, independent of the N_H assumed. Sufficient uncertainty exists in the data to allow some other extragalactic spectrum to produce this agreement, but the minimum extragalactic intensity required to allow a fit consistent with a thermal plasma model is 20 cts s^{-1} in the I band (~0.85–1.15 keV) alone.

With the temperature of one component determined by the MI band-fraction diagram, the temperature of the other component is defined by the requirement that the two components reproduce the observed BCM band-fraction point. Figure 7 is a BCM band-fraction diagram on which are plotted band-fraction values appropriate to RS model spectra, labeled by the logarithm of the temperature. The solid line assumes $N_H = 0$, while the dashed line indicates how the band-fractions change for a particular RS model spectrum (log $T = 6.4$) as the amount of intervening absorption is increased. A straight line originating at the log $T = 6.4$, $N_H = 3 \times 10^{20}$ cm^{-2} model band-fraction point in Figure 7 and passing through the data point for direction R intersects the model spectrum line near log $T = 6.0$. Hence, to reproduce the observed band ratios, the RS model for the low-temperature region has log $T \approx 6.0$. Table 3 gives the temperatures and emission measures derived using band fraction data for directions R and T and the band efficiency curves of Figures 8 and 9. These parameter values are insensitive to the exact value of N_H assumed for the fits.

VII. DISCUSSION AND CONCLUSIONS

The spatial structure of the 0.5–1.2 keV (MI band) diffuse X-ray intensity at latitudes $b < -15°$ consists of several extended features imposed on a relatively uniform background. The extended features, one in the Eridanus region and one in the direction of the galactic center, are most likely the result of supernova explosions, but we do

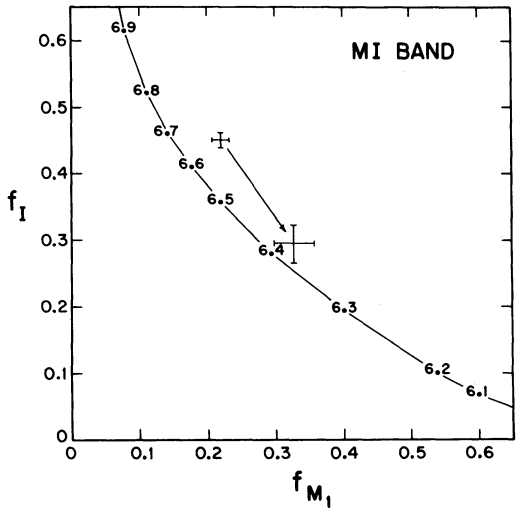

FIG. 6

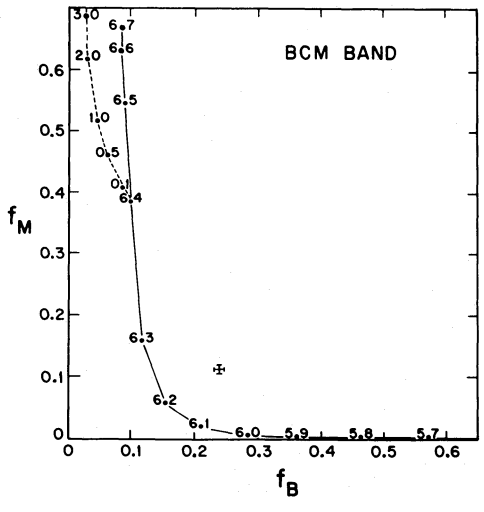

FIG. 7

FIG. 6.—MI band-fraction diagram. The solid line indicates the band-fraction points calculated from a Raymond and Smith (1979) thermal plasma model spectrum and is labeled by the logarithm of the temperature. The upper data point is derived from the measured rates from point R ($l \sim 284°$, $b \sim -79°$). The lower data point represents point R after subtraction of the absorbed 11 $E^{-1.4}$ spectrum from the data. Error bars are 1 σ.

FIG. 7.—BCM band-fraction diagram. The solid line indicates the band-fraction points calculated from a Raymond and Smith (1979) thermal plasma model spectrum and is labeled by the logarithm of the temperature. The dashed line indicates how the band-fractions change for a log $T = 6.4$ spectrum as the amount of intervening absorption is increased. The dashed line is labeled by N_H in units of 10^{20} cm^{-2}. The data point corresponds to the data from point R after subtraction of the absorbed 11 $E^{-1.4}$ spectrum. Error bars are 1 σ.

TABLE 3

RESULTS OF BAND FRACTION FITS

	HIGH-TEMPERATURE COMPONENT		LOW-TEMPERATURE COMPONENT	
POINT	T (K)	$n_e^2 d$ (cm^{-6} pc)	T (K)	$n_e^2 d$ (cm^{-6} pc)
R	$10^{6.4}$	0.004	$10^{6.0}$	0.003
T	$10^{6.4}$	0.004	$10^{6.0}$	0.002

not rule out a contribution from the galactic center itself. Apart from these features, the uniform background, present at an intensity higher than an extrapolation of the 2–10 keV background, admits several interpretations.

The spatial model for the general MI band diffuse background that most nearly resembles the data is that of an unabsorbed isotropic intensity. Such a flux would have to originate fairly locally (closer than ~ 100 pc), but there are problems in accommodating a totally local isotropic origin (§ III). Two other spatial models that resemble the data almost as well are both two-component models of which the first component is an absorbed extragalactic 11 $E^{-1.4}$ spectrum, which supplies 50–60% of the MI band count rate. The second component in one case (Model I) is isotropic and unabsorbed, and in the other case (Model III) the second component is disk-shaped and absorbed by galactic gas so that the increased absorption at low galactic latitudes balances the increased emission in those directions.

The isotropic unabsorbed component of Model I, which provides $\sim 40\%$ of the MI band flux, has the advantage of simplicity but requires a fortuitous location

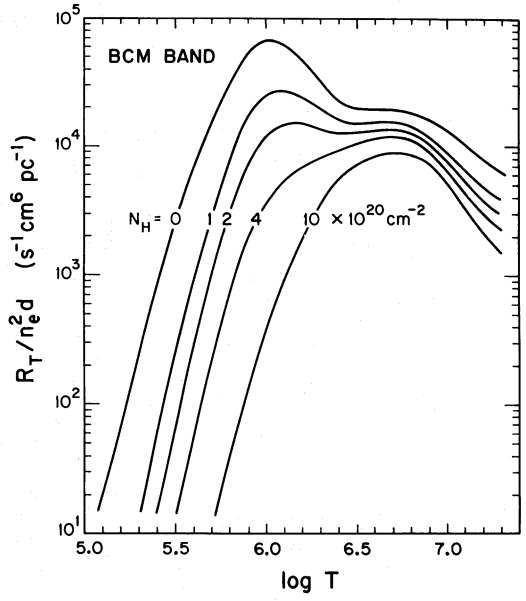

FIG. 8.—Calculated curves of the total count rate in the B, C, and M bands per unit emission measure from a single temperature emitting region. Different curves are labeled by the column density of intervening neutral matter. Raymond and Smith (1979) model spectra are used.

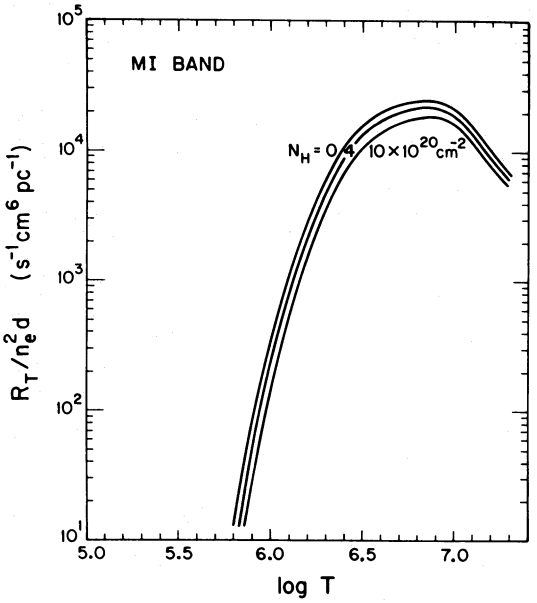

FIG. 9.—Same as Fig. 8, but for M_1, M_2, and I bands

of the Sun (see § III). An alternative interpretation of Model I, galactic emission distributed spatially with the galactic absorbing material (Davidsen *et al.* 1972), is also difficult to accommodate. Consequently, we do not favor the Model I picture.

A physical interpretation of the absorbed, disk-shaped component of Model III is easier to accommodate. A number of authors (e.g. Spitzer 1956; Shapiro and Field 1976; Chevalier and Oegerle 1979; Bregman 1979; Cox 1981) have discussed models of a hot galactic halo. Savage and de Boer (1979, 1981) have observed high-excitation interstellar absorption lines which they interpret as evidence for a hot galactic halo. Emission from such a halo would resemble the disklike component of Model III. Alternatively, Rosner *et al.* (1981) have derived an X-ray luminosity function for M stars and suggest that the stellar contribution to the high-latitude diffuse X-ray background in the MI band may be as much as 30%. A large scale height stellar population of emitters would also resemble the disklike component of our Model III. We favor the Model III spatial picture, but do not differentiate a hot gaseous disk-shaped halo from a disklike distribution of M stars.

Next we consider the spectral characteristics of the data. Independent of specific spectral models, the variation of the B, C, M_1, M_2, and I band data with N_H is consistent with a simple picture in which all of the B band, most of the C band, and almost none of the MI band photons originate in a region *closer* to the Sun than most the galactic absorbing gas. In this picture, all of the MI band intensity and the remainder of the C band intensity originate *beyond* the galactic absorbing gas. When the data are compared to specific spectral models, the pulse height distribution of the MI band radiation is consistent with an 11 $E^{-1.4}$ spectrum plus a $T \sim 10^{6.4}$

K RS spectrum, both absorbed by all the neutral material along the line of sight. The B and C band data are consistent with an additional $T \sim 10^6$ K unabsorbed RS spectrum.

We interpret the cooler component, the region closer to the Sun than practically all the absorbing galactic gas, as the region suggested by Sanders *et al.* (1977) and by Fried *et al.* (1980) to explain the B and C band data. The hotter, $T \sim 10^{6.4}$ K, emission we associate with the disk-shaped component of spatial Model III. (The $T \sim 10^{6.4}$ K emission would correspond to the isotropic component of spatial Model I.) Thus both spatial and spectral data are consistent if the soft X-ray background results from the combination of three sources: a local region of irregular geometry with $T \sim 10^6$ K, a continuation of the 11 $E^{-1.4}$ photons cm^{-2} s^{-1} sr^{-1} keV^{-1} extragalactic spectrum to energies $\sim$0.5 keV, and a disklike galactic halo with emission characterized by $T \sim 10^{6.4}$ K. Whether this latter emission arises from dispersed hot gas or from a population of stars, the observations in direction R yield an effective emission measure perpendicular to the plane of the disk $n_e{}^2 d \sim 4 \times 10^{-3}$ cm^{-6} pc, which corresponds to an energy flux of $F \sim 1.2 \times 10^{-8}$ ergs cm^{-2} s^{-1} sr^{-1} in the band 0.5–1.2 keV.

If the $\sim 10^{6.4}$ K emission arises from stellar sources with average luminosity L, space density in the galactic plane n, and scale height λ, the energy flux is $F = Ln\lambda/4\pi$. With $n = 0.065$ pc^{-3} and $\lambda = 350$ pc, appropriate to dM stars (Allen 1973), the required average luminosity in the 0.5–1.2 keV band is 8×10^{28} ergs s^{-1}. This mean luminosity is of the same order of magnitude as the mean luminosity of dM stars as deduced from *Einstein* results by Rosner *et al.* (1981). If the $10^{6.4}$ K emission arises from hot dispersed gas, the pressure ($P/k = 2n_eT$) would be $\sim 10^4$ cm^{-3} K if the region extends to 1 kpc.

Our view of the hot interstellar medium differs from that of Hayakawa *et al.* (1978) and Inoue *et al.* (1979). Their view is that the Sun is surrounded by a single-temperature local region with $T \sim 10^{6.2}$ K, and they find no evidence for another galactic component. Their view is based on fits to their pulse height data, combined with the observation by Hayakawa *et al.* of a constant M/L (M band to C band) ratio from the sky not including loops I and II. Our data are not consistent with their view. Figures 3, 4, and 5 of Fried *et al.* (1980) show that our data do not support a constant M band to C band ratio outside loops I and II in the southern galactic hemisphere. Spectral fits to both our pulse height data (Fried *et al.*) and our broad band data (this paper) always produce much better fits to a two-temperature model than to a single-temperature one, independent of whether Kato (1976) or RS model spectra are used. We cannot be sure of the cause of the discrepancy, but we suspect it lies in the greater spectral separation afforded by our boron-coated and Kimfol windows. Our data seem capable of eliminating models that their data cannot.

This research was supported by the National Aeronautics and Space Administration under grant NGL 50-002-044. The authors thank Dave Burrows, Alan Bunner, Don Cox, and Dan McCammon for helpful discussions. Rick Borken, Paul Burstein, DeAnn Iwan, Pat LaMaster, Tim Quigley, and Fred Williamson participated in the data reduction and analysis. For their excellent support we thank the Sounding Rocket Branch of the Goddard Space Flight Center, the launch crews of the US Navy at White Sands Missile Range, and the launch crew of the Australian Rocket Range at Woomera.

REFERENCES

Allen, C. W. 1973, *Astrophysical Quantities* (3d ed.; London: Athlone Press).
Berkhuijsen, E. M. 1973, *Astr. Ap.*, **24**, 143.
Borken, R. J., and Iwan, D. C. 1977, *Ap. J.*, **218**, 511.
Bregman, J. N. 1980, *Ap. J.*, **236**, 577.
Brown, R. L., and Gould, R. J. 1970, *Phys. Rev. D*, **1**, 2252.
Bunner, A. N., Coleman, P. L., Kraushaar, W. L., and McCammon, D. 1971, *Ap. J.* (*Letters*), **167**, L3.
Bunner, A. N., Sanders, W. T., and Nousek, J. A. 1979, *Ap. J.* (*Letters*), **228**, L29.
Burstein, P., Borken, R. J., Kraushaar, W. L., and Sanders, W. T. 1977, *Ap. J.*, **213**, 405.
Chevalier, R. A. 1974, *Ap. J.*, **188**, 501.
Chevalier, R. A., and Oegerle, W. R. 1979, *Ap. J.*, **227**, 398.
Cleary, M. N., Heiles, C., and Haslam, C. G. T. 1979, *Astr. Ap. Suppl.*, **36**, 95.
Cox, D. P. 1981, *Ap. J.*, **245**, 534.
Cox, D. P., and Anderson, P. R. 1982, *Ap. J.*, **253**, 268.
Cox, D. P., and Smith, B. W. 1974, *Ap. J.* (*Letters*), **189**, L105.
Davidsen, A., Shulman, S., Fritz, G., Meekins, J. F., Henry, R. C., and Friedman, H. 1972, *Ap. J.*, **177**, 629.
Dickey, J. M., Salpeter, E. E., and Terzian, Y. 1979, *Ap. J.*, **228**, 465.
Fried, P. M., Nousek, J. A., and Garmire, G. P. 1982, in preparation.
Fried, P. M., Nousek, J. A., Sanders, W. T., and Kraushaar, W. L. 1980, *Ap. J.*, **242**, 987.
Gorenstein, P. 1975, *Ap. J.*, **198**, 95.
Hayakawa, S., Iwanami, H., Kuneida, H., Nagase, F., and Yamashita, K. 1979, in *X-ray Astronomy*, ed. W. A. Baity and L. E. Peterson (Oxford: Pergamon).
Hayakawa, S., Kato, T., Nagase, F., Yamashita, K., Murakami, T., and Tanaka, Y. 1977, *Ap. J.* (*Letters*), **213**, L109.
Hayakawa, S., Kato, T., Nagase, F., Yamashita, K., and Tanaka, Y. 1978, *Astr. Ap.*, **62**, 21.
Heiles, C. 1976, *Ap. J.* (*Letters*), **208**, L137.
Henry, R. C., Fritz, G., Meekins, J. F., Chubb, T., and Friedman, H. 1971, *Ap. J.* (*Letters*), **163**, L73.
Inoue, H., Koyama, K., Matsuoka, M., Ohashi, T., Tanaka, Y., and Tsunemi, H. 1979, *Ap. J.* (*Letters*), **227**, L85.
———. 1980, *Ap. J.*, **238**, 886.
Iwan, D. C. 1980, *Ap. J.*, **239**, 316.
Kato, T. 1976, *Ap. J. Suppl.*, **30**, 397.
Naranan, S., Schulman, S., Friedman, H., and Fritz, G. 1976, *Ap. J.*, **208**, 718.
Paresce, F., and Stern, R. 1981, *Ap. J.*, **247**, 89.
Raymond, J. C., and Smith, B. W. 1979, private communication (RS).
Reynolds, R. J., and Ogden, P. M. 1979, *Ap. J.*, **229**, 942.
Ride, S. K., and Walker, A. B. C. 1977, *Astr. Ap.*, **61**, 347.
Rosner, R., *et al.* 1981, *Ap. J.* (*Letters*), **249**, L5.
Sanders, W. T., Kraushaar, W. L., Nousek, J. A., and Fried, P. M. 1977, *Ap. J.* (*Letters*), **217**, L87.
Savage, B. D., and de Boer, K. S. 1979, *Ap. J.* (*Letters*), **230**, L77.
———. 1981, *Ap. J.*, **243**, 460.

Seward, F., Burginyon, G., Grader, R., Hill, R., Palmieri, T., Stoering, P., and Toor, A. 1976, *Ap. J.*, **205**, 238.
Shapiro, P. R., and Field, G. B. 1976, *Ap. J.*, **205**, 762.
Shapiro, P. R., and Moore, R. T. 1976, *Ap. J.*, **207**, 460.
Spitzer, L. 1956, *Ap. J.*, **124**, 40.
Stern, R., and Bowyer, S. 1979, *Ap. J.*, **230**, 755.
Weaver, H. F. 1979, in *Proc. IAU Symposium 84, The Large-Scale Characteristics of the Galaxy*, ed. W. B. Burton (Dordrecht: Reidel), p. 295.
Williamson, F. O., Sanders, W. T., Kraushaar, W. L., McCammon, D., Borken, R. J., and Bunner, A. N. 1974, *Ap. J.* (*Letters*), **193**, L133.

P. M. FRIED: 4C-224A, Bell Laboratories, Whippany Road, Whippany, NJ 07981

W. L. KRAUSHAAR and W. T. SANDERS: Department of Physics, University of Wisconsin, Madison, WI 53706

J. A. NOUSEK: Department of Astronomy, 503 Davy Lab, Penn State, University Park, PA 16802